Identification of the Tumor Boundary of Hilar Cholangiocarcinoma Based on Multiphoton Microscopy

Huiling Zhan, Caihong Sun, Tianyi Luo, Gangqin Xi, Yikun Guo, Mingyu Xu, Youting Chen, and Shuangmu Zhuo

***Abstract*—Hilar cholangiocarcinoma (HCC) is a common malignant tumor of the biliary system. The structural characteristics of the bile duct tissue can reflect the changes in its function. The visualization of these specific features is of special significance for understanding the degree of invasion of HCC and tumor borders. Radical R0 resection is the only cure for HCC. Currently, the commonly used medical imaging diagnostic methods can only provide a rough tumor range and require a histopathological analysis. Multiphoton microscopy (MPM) not only has an ultra-high spatial resolution but is also extremely sensitive to collagen fibers with noncentrosymmetric structures. In this study, MPM is applied to image the boundaries of HCC tumors. First, the experimental results show that MPM can clearly reveal the existence of residual cancer cells at the surgical margin. Second, the density of the collagen fibers and the dispersion of the 2D direction angle of the collagen fibers of normal and cancerous tissues are further calculated quantitatively. The collagen fiber signals before and after cancer cell invasion into the different tissues are found to be different. Finally, through a logistic regression prediction curve, combined with the collagen fiber density and 2D direction angle as indicators, it is further judged whether the resection margin is negative, which is closely related to the prognosis of HCC. The experimental results indicate that MPM imaging can serve as a new tool for diagnosing whether the HCC tumor boundary reaches R0 resection.**

***Index Terms*—Multiphoton microscopy, hilar cholangiocarcinoma, tumor boundary, collagen.**

I. Introduction

HILAR cholangiocarcinoma (HCC) is a malignant tumor caused by bile duct epithelial cell lesions [1], [2]. It is a relatively common type of extrahepatic cholangiocarcinoma (ECC), accounting for approximately 60%–70% of ECC [3]. Hence, it is of great significance to accurately understand the infiltration process of cancer tissue and completely remove the tumor. Invasive metastasis is one of the more common ways of metastasis in HCC, and cancer cells mostly grow diffusely, infiltrating the bile duct wall. The hilar bile duct tissue is partially surrounded by the liver. When cancer cells infiltrate and metastasize, they first enter the muscularis propria from the mucosal layer and then directly reach the liver. This is because the extrahepatic bile duct does not have a well-developed serous membrane like most gastrointestinal tracts [4]. As patients with HCC often do not have evident clinical symptoms at an early stage, when progressive painless obstructive jaundice occurs, most of them would have entered the advanced stage. Many studies have shown that radical resection of the tumor tissue is the only cure [5], [6], [7]. Therefore, we should determine the exact location of the tumor based on the preoperative and intraoperative evaluation of the tumor to ensure that the surgical margin is negative as much as possible, so as to reduce the recurrence rate and improve the survival rate. Currently, the preoperative evaluation methods for hepatic hilar include computed tomography (CT), endoscopic retrograde cholangiography (ERC), ultrasound (US), and magnetic resonance imaging (MRI) [8], [9]. Unfortunately, these methods can only provide the approximate scope of the tumor. Because there is no histological analysis, it is impossible to ensure that the operation can achieve R0 resection. The conventional frozen section has a long production process [10], and errors can be easily produced when the doctor is inexperienced. More research is required to find new ways to ensure that the negative margin is achieved.

Multiphoton microscopy (MPM) based on second harmonic generation (SHG) and two-photon excitation fluorescence (TPEF) is a rapid microscopy imaging technology with a high spatial resolution [11]. Significant developments have been made in multiphoton endoscopes, which have been used for in vivo mouse model imaging [12], [13]. MPM is a rapid microscopic imaging technique with less phototoxicity and photobleaching, high spatial resolution, and large imaging depth to tissues. In the imaging process, the SHG and TPEF images of the tissue can be obtained without staining, and the structure and function information of the tissue can be further obtained through analysis. Currently, the MPM has been widely used in the imaging of gastric cancer [14], bowel cancer [15], breast

Manuscript received 10 May 2022; revised 29 July 2022; accepted 28 August 2022. Date of publication 5 September 2022; date of current version 13 September 2022. This work was supported in part by the National Key Research and Development Program of China under Grant 2019YFE0113700, in part by the Natural Science Foundation of Fujian Province under Grant 2021J01431, in part by the Young and Middle-aged Key Personnel Training Project of Fujian Provincial Health Commission under Grant 2018-ZQN-44, and in part by the Joint Funds of Fujian Provincial Health and Education Research under Grant 2019-WJ-21. *(Huiling Zhan and Caihong Sun contributed equally to this work.) (Corresponding authors: Shuangmu Zhuo; Youting Chen.)*

Huiling Zhan, Caihong Sun, Tianyi Luo, Gangqin Xi, Mingyu Xu, and Shuangmu Zhuo are with Jimei University, Xiamen, Fujian 361020, China (e-mail: 310088276@qq.com; 37163257@qq.com; 2651485278@qq.com; xigangqin@jmu.edu.cn; 825210378@qq.com; shuangmuzhuo@gmail.com).

Yikun Guo and Youting Chen are with Fujian Medical University, Fuzhou, Fujian 350108, China (e-mail: 1165307317@qq.com; chenyt1381@163.com).

This work involved human subjects or animals in its research. Approval of all ethical and experimental procedures and protocols was granted by the Institutional Review Committee of the First Affiliated Hospital of Fujian Medical University.

Digital Object Identifier 10.1109/JPHOT.2022.3203511

cancer [16], and other diseases. The above studies have laid a foundation for the early application of MPM to human bile duct tissue to judge tumor boundaries.

Combining the characteristics of HCC and advantages of MPM, we aim to detect HCC at the tumor border using MPM to achieve R0 resection. Therefore, we analyzed the tumor margins of HCC from two perspectives. First, the SHG/TPEF and H&E images were qualitatively analyzed. Second, two quantitative indicators were obtained from the SHG images, which were used for the quantitative analysis of HCC.

In this study, we use MPM to detect cancer tissues at the border of the tumor. We demonstrate that MPM imaging can help observe the tissue structure and cell morphology of the HCC tumor boundary and help determine whether the tumor boundary reaches R0 resection through quantitative and qualitative methods. The qualitative analysis of the image in terms of the histomorphology shows that the multiphoton image can more quickly and conveniently help determine the tumor boundary location. At the border of the tumor, two indicators, namely the density of the collagen fibers and the dispersion of the 2D direction angle, are quantitatively calculated. When cancer cells infiltrate the muscle layer, the collagen fiber signal content is significantly reduced; however, when the cells infiltrate the liver, the content increases due to fibrotic reactions. Combining the density of the collagen fibers and 2D direction angle, a logistic regression prediction curve is drawn. Compared with a single quantitative indicator, the prediction curve is more beneficial to the diagnosis of the tumor boundary. Therefore, MPM imaging can quantitatively diagnose the state of HCC tumor borders.

II. Materials and Methods

A. Sample Preparation

In this study, samples were collected from the First Affiliated Hospital of Fujian Medical University (Fuzhou, China) from 2018 to 2020, including three cases of normal bile duct tissue, eight cases of HCC (four cases of cancer cells infiltrating the muscular layer of the bile duct and four cases of cancer cells passing through the muscular layer to reach the liver). This study was approved by the Institutional Review Committee of the First Affiliated Hospital of Fujian Medical University, and the patients provided written informed consent.

To clearly show our experimental results and prove that MPM can be used for tumor boundary assessment, we used a microtome to continuously slice each specimen into five slices, each with a thickness of 5 microns. The middle slice was used for hematoxylin and eosin (H&E) staining, and the remaining four slices were used for multiphoton microscopy (tumor border). Each sample was placed on a glass slide and sealed by a cover glass. To improve the quality of multiphoton imaging and prevent dehydration and shrinkage of the sample, a small amount of phosphate-buffered saline solution can be used on the sample. The multiphoton and H&E images were compared and analyzed by two certified pathologists.

B. Multiphoton Microscopic Imaging System

The multiphoton microscopy imaging system is composed of a laser scanning microscope Axio Examiner Z1 (Zeiss LSM 880, Jena, Germany) and an external mode-locked Ti:Sapphire laser (140 fs, 80 MHz); the adjustable range is 680–1080 nm [17]. In this experiment, we used excitation light with a wavelength of 810 nm. The emitted fluorescence was spectrally separated by a grating to the optimized 32-channel photomultiplier tube (PMT) array detector, and the SHG and TPEF signals were then collected by the PMT detector. The wavelength range for collecting the SHG signals was 390–420 nm, marked with pseudo-color green. The wavelength range for collecting the TPEF signal was 430–650 nm, marked with pseudo-color red. To collect images with a wider range, we used Plan-Apochromat $20\times$ (NA $= 0.8$) objective (Zeiss). If a certain area of interest needs to be enlarged, we can directly switch to a Plan-Apochromat $63\times$ (NA $= 1.4$) oil immersion objective (Zeiss). All the images had an eight-bit pixel depth and were obtained by bidirectional scanning. All the images were obtained under the same conditions.

C. Quantitative Analysis

The changes in the collagen fibers in HCC are closely related to the degree of cancer cell invasion, which is of great significance for determining the tumor boundary. To quantitatively describe the changes in the structural characteristics of the tumor boundary after cancer cells invade the muscle layer and the liver, we mainly performed a quantitative analysis of the collagen fiber density and 2D direction angle of the tumor boundary. In each tissue sample, six regions of interest of the same size were selected, totaling 24 spots where cancer cells infiltrate the bile duct muscle layer and 24 spots where cancer cells infiltrate the liver.

When calculating the density of the collagen fibers, we used MATLAB to binarize the image, where the white area corresponds to the SHG signal. The ratio of white area pixels to the total pixels is the value of the collagen density. When calculating the 2D direction angle of the collagen fibers, we used an automatic tracking algorithm called CT-FIRE to extract the collagen fibers [18], and the data were calculated using MATLAB. CT-FIRE is a combination of a curve-denoising filter and FIRE algorithm [18]. First, we use the curve-denoising filter to process an SHG image. Next, the FIRE algorithm starts with the application of thresholds to form a binary image to distinguish between the fiber and background pixels. Then, MATLAB is used to calculate the minimum distance between the binary fiber and background pixels. Next, the maximum ridge is tracked along the distance function. After each nuclear point is extended to form a fiber branch, the short fiber branch is built. Finally, the fiber length and direction are obtained and connected with adjacent fibers [19]. We used IBM SPSS Statistics 24.0 for the data analysis, and the results were presented in the form of mean plus standard deviation. Finally, we used MedCalc to draw the receiver operating characteristic (ROC) curve.

III. Results and Discussion

A. Normal Hilar Bile Duct Tissue

Fig. 1 shows the SHG/TPEF and corresponding H&E images of the normal hilar bile duct tissue and adjacent liver tissues. Clearly, the mucosal layer is composed of a single layer of tall columnar epithelial cells (blue arrow), and then down into

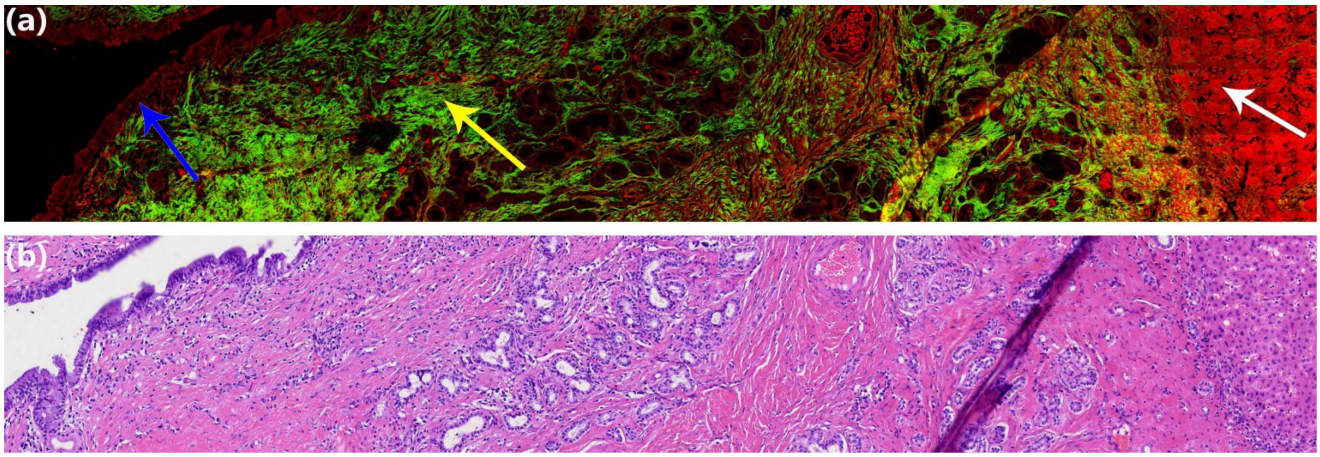

Fig. 1. Comparison of overlaid SHG/TPEF and corresponding H&E-stained images of normal hilar bile duct tissue. (a) Typical overlaid SHG/TPEF image (63×) of an unstained section: mucosal layer (blue arrow), muscle layer (yellow arrow), and liver (white arrow). (b) Corresponding H&E-stained image.

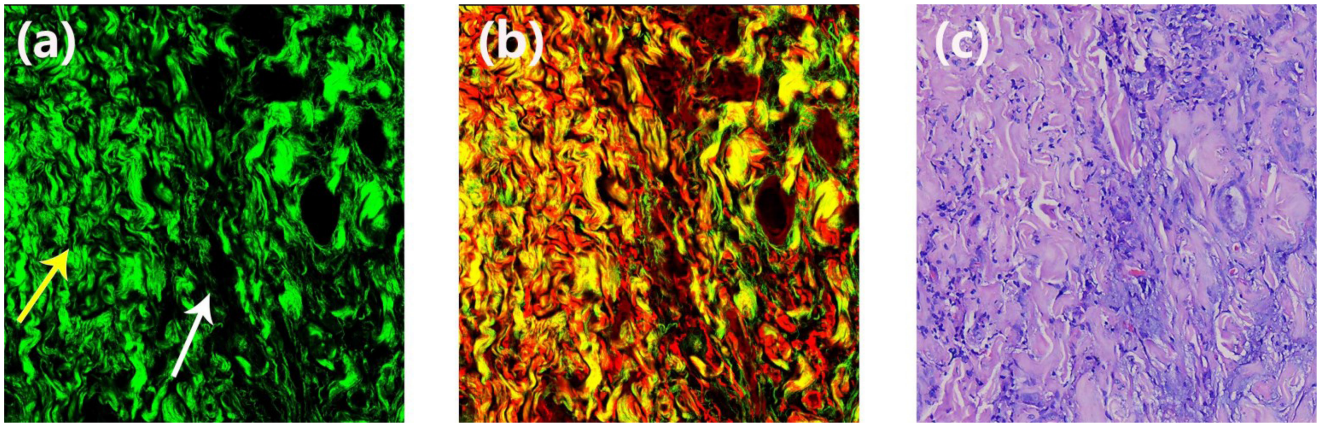

Fig. 2. Comparison of SHG, overlaid SHG/TPEF, and corresponding H&E-stained images of hilar cholangiocarcinoma where cancer cells infiltrate the muscle layer. (a) Typical SHG image (63×) of an unstained section. (b) Typical overlaid SHG/TPEF image (63×) of an unstained section. Normal tissue on the left, cancerous tissue on the right. (c) Corresponding H&E-stained image.

the muscle layer, we find rich dense connective tissue (yellow arrow). The muscle layer is mainly composed of collagen and elastic fibers, which also contain various blood vessels, nerves, and mucous glands around the bile duct [20]. When the tissue becomes cancerous, these can become one of the ways for cancer cells to metastasize. Continuing down to enter the liver (white arrow), the liver contains fewer collagen fibers than the muscle layer.

B. Tumor Boundary of Hilar Cholangiocarcinoma

Fig. 2 shows the SHG, SHG/TPEF, and corresponding H&E images of the tumor boundary after cancer cells invade the muscle layer. The collagen fibers of the normal muscle layer are relatively thick, which are very close to each other, showing small waves (yellow arrow). When cancer cells infiltrate the muscle layer, first, the collagen fibers become loose, and their density drops sharply. Second, the shape of the collagen fibers changes from the original small waves to irregularly curved. The collagen fibers become narrower and are no longer thick (white arrow). Part of the reason for these changes in the collagen fibers is that the cancer cells can produce matrix metalloproteinase-9 (MMP-9), which can promote the infiltration and metastasis of the cancer cells by degrading collagen [21]. More importantly, MMP-9 is not expressed or lowly expressed in benign bile duct tissues, whereas it is highly expressed in cholangiocarcinoma [22]. Although the cell structure in the H&E image is the same as that in the multiphoton image, it is difficult to distinguish the tumor boundary after the cancer cells have invaded the muscle layer in the H&E image.

Fig. 3 shows the SHG, SHG/TPEF, and the corresponding H&E images at the junction of the mucinous glands around the cancerous bile duct and the muscular connective tissue. The epithelial cells of the mucous glands around the bile duct are one of the origins of HCC [2], [23], [24]. The figure clearly shows that the mucous glands around the bile duct are twisted and deformed [25]. Some cancer cells float in the mucous lake inside the glands, forming cancer nests (blue arrow). Other

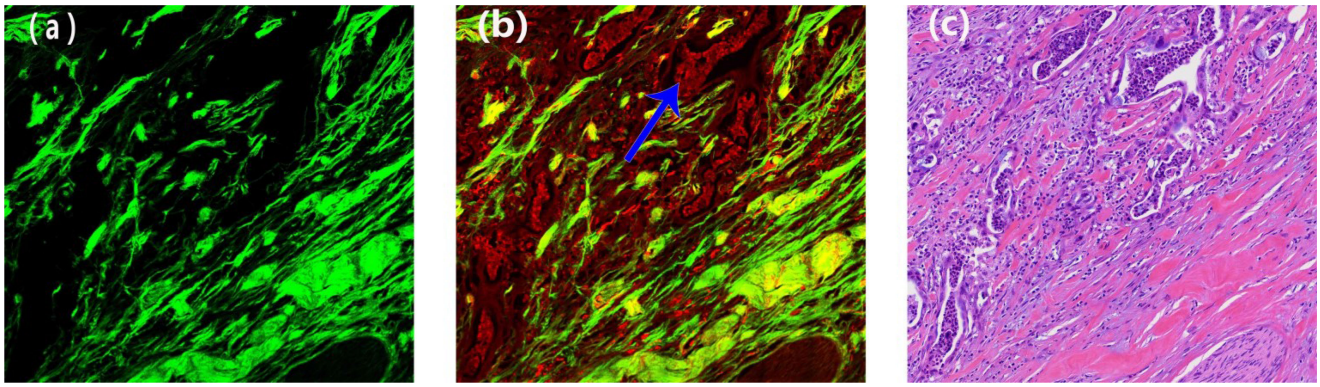

Fig. 3. Comparison of SHG, overlaid SHG/TPEF, and corresponding H&E-stained images of hilar cholangiocarcinoma where cancer cells are in the mucous glands around the bile duct. (a) Typical SHG image (63×) of an unstained section. (b) Typical overlaid SHG/TPEF image (63×) of an unstained section, cancer nests (blue arrow). (c) Corresponding H&E-stained image.

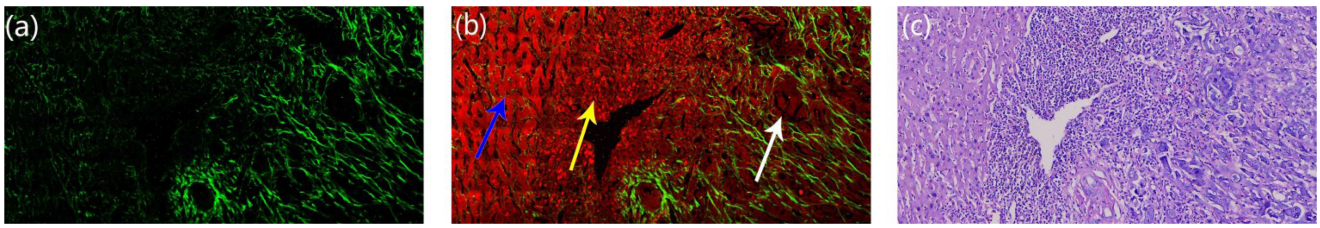

Fig. 4. Comparison of SHG, overlaid SHG/TPEF, and corresponding H&E-stained images of hilar cholangiocarcinoma where cancer cells infiltrate the liver. (a) Typical SHG image (63×) of an unstained section, distinctly revealing the tumor boundary. (b) Typical overlaid SHG/TPEF image (63×) of an unstained section: normal liver plate (blue arrow), inflammatory cells (yellow arrow), and cancer cells (white arrow). (c) Corresponding H&E-stained image.

cancer cells that infiltrate the connective tissues are ready to spread to normal tissues. The morphological difference between the mucinous glands around the cancerous bile duct and the surrounding normal connective tissue is quite different. In the connective tissue infiltrated by cancer cells, the collagen fibers become slender, and the density is reduced, which is in sharp contrast with normal collagen fibers, and the tumor boundary is easier to distinguish. Compared with the H&E image, we can not only observe the cell structure characteristics from the multiphoton image, but can also judge the boundary of the tumor from the change in the collagen. Thus, the multiphoton map is more advantageous.

Fig. 4 shows the SHG, SHG/TPEF, and corresponding H&E images at the tumor boundary after the cancer cells invade the liver. The left side of the image shows normal liver tissue, and the collagen around the liver cells is arranged in an orderly manner, showing a tiny mesh structure [26]. The middle of the image is the junction of the cancerous and normal tissues. The junction is filled with inflammatory cells produced by inflammation. The normal liver cells are arranged to form a spongy liver plate (blue arrow). Inflammatory cells are regular and granular (yellow arrow), while cancer cells are of different shapes and sizes, showing evident pleomorphism (white arrow). It is easier to distinguish the liver plate, inflammatory cells, and cancer cells. Moreover, the collagen fibers at the junction start to scatter. The liver tissue on the right side of the image is infiltrated by the cancer cells. The most prominent feature is that the collagen fibers increase in number due to the fibrotic reaction [27], [28]

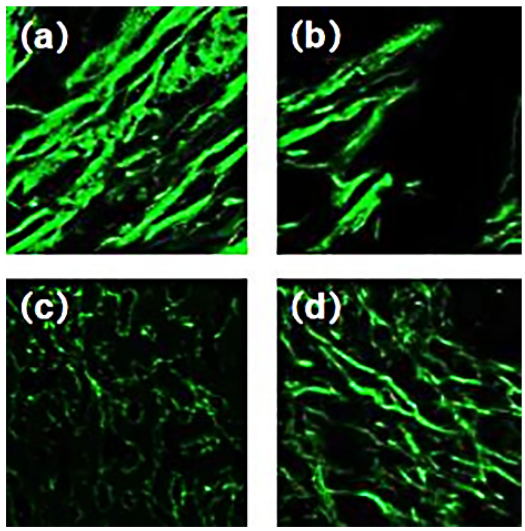

Fig. 5. Typical SHG images of the tumor boundary taken from Figs. 2 and 4. (a) Normal collagen fibers in the muscle layer. (b) Cancerous collagen fibers in the muscle layer. (c) Normal collagen fibers in liver. (d) Cancerous collagen fibers in the liver.

and become thick; however, the structure is disorderly. The above changes in the collagen is not reflected in the H&E image. Although the cell structure in the H&E image is the same as that in the multiphoton image, it is more convenient and faster to judge the tumor boundary based on the change in the collagen

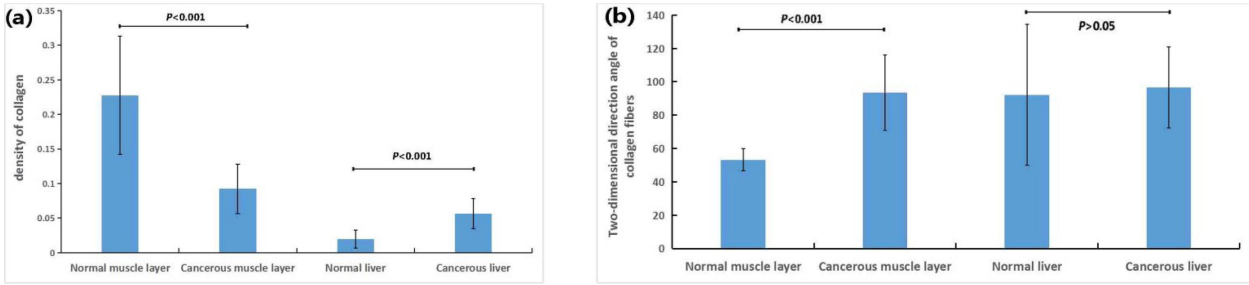

Fig. 6. Infiltration of cancer cells into the muscle layer and liver. (a) Density of collagen fibers at the tumor border. (b) Two-dimensional direction angle of the collagen fibers at the tumor border. Error bars indicate the standard deviation.

fibers in the SHG image. Therefore, a diagnosis based on the multiphoton image will be better than that based on the H&E image.

C. Quantitative Assessment of Normal and Cancerous Tissues At the Tumor Border

The boundary state is one of the most reliable predictors of long-term survival. We not only describe the morphology of the tumor boundary from a qualitative perspective, but also quantitatively explain the changes in the collagen fibers at the tumor boundary in terms of the collagen fiber density and the dispersion of the 2D orientation angle. Finally, a judgment on the tumor boundary is made.

When cancer cells infiltrate the muscle layer, Figs. 5(a) and 5(b) show evident changes in the collagen fibers. As shown in Fig. 6, the density of the collagen fibers in the normal muscle layer is 0.228 ± 0.085 ($N = 24$); however, in the muscle layer infiltrated by cancer cells, the density decreases to 0.092 ± 0.037 ($N = 24$). There is a significant statistical significance between the two groups of data ($p < 0.001$). As the sample size increases, the standard deviation becomes more accurate [29]. Accordingly, a larger standard deviation indicates that our data is scattered. The 2D direction angle of the collagen fibers in the normal muscle layer is 53.247 ± 6.525 ($N = 24$). However, after being invaded by the cancer cells, the collagen fibers no longer bend regularly, the data is scattered, and their 2D direction angle becomes 93.390 ± 22.600 ($N = 24$). Similarly, there is significant statistical significance between the two sets of data ($p < 0.001$).

When the cancer cells infiltrate the liver, Figs. 5(c) and 5(d) show another change in the collagen fibers. As shown in Fig. 6, the density of the collagen fibers in the normal liver is 0.020 ± 0.013 ($N = 24$). However, the density of the collagen fibers increases and becomes 0.056 ± 0.022 ($N = 24$) after being infiltrated by the cancer cells. There is a significant statistical significance between the two sets of data ($p < 0.001$). The 2D direction angle of the collagen fibers in the normal liver is 92.162 ± 42.211 ($N = 24$). Therefore, the angle measurements in normal livers are scattered. After cancer cell infiltration, the 2D direction angle of the collagen fibers does not change significantly; the value is 96.663 ± 24.262 ($N = 24$). Although there is no statistical significance between the two sets of data ($p > 0.05$), the standard deviation of the cancerous liver angle measurement is smaller than the normal one. Therefore, when the sample size is the same, the angle measurement data of the cancerous liver are more concentrated.

If the above two quantitative indicators (collagen fiber density and the dispersion of 2D direction angle) are used as an indicator to judge the presence of residual cancer tissue, the judgment result of the 2D orientation angle alone is not obvious. Even if the standard deviation analysis of the 2D direction angle is added, it can only roughly reflect the change in dispersion. Therefore, to fully reflect whether the tumor margin reached R0 resection or not, we hope that more information can be obtained by combining the collagen fiber density and 2D orientation angle.

D. Tumor Boundary Prediction Curve

Through the above analysis, to more accurately evaluate the boundary state of the tumor, we performed logistic regression on the density of the collagen fibers and the 2D direction angle and obtained corresponding coefficients A1, A2, and a constant c. Subsequently, we plot a prediction curve that combines the density of the collagen fibers and the 2D direction angle. The predicted value $= c + A1 * \text{collagen fiber density} + A2 * \text{collagen fiber 2D direction angle}$.

We draw the ROC curve of the collagen fiber density, 2D direction angle, and predicted value in the case when the cancer cells enter the muscle layer or liver. When the cancer cells infiltrate the liver, as shown in Fig. 7(b), the result obtained by the prediction curve (AUC = 0.965) is better than those obtained by the collagen fiber density (AUC = 0.962) and 2D orientation angle (AUC = 0.553). When the cancer cells infiltrate the muscle layer, as shown in Fig. 7(a), the results obtained by the prediction curve (AUC = 0.956) and those obtained by the collagen fiber density (AUC = 0.957) are approximately the same. This result is superior to the result of the 2D orientation angle (AUC = 0.637). The tumor boundary can still be distinguished well. However, because the sample size is too small, the predicted value is not significantly improved. When the sample size (the data quantity of the whole experiment) is sufficiently large, the predicted value is significantly better, making our results more generalizable [30]. The above shows that compared to quantifying a feature alone, it is more accurate to use a prediction curve that combines the density and 2D direction angle of the collagen fibers to determine whether the tumor boundary is negative.

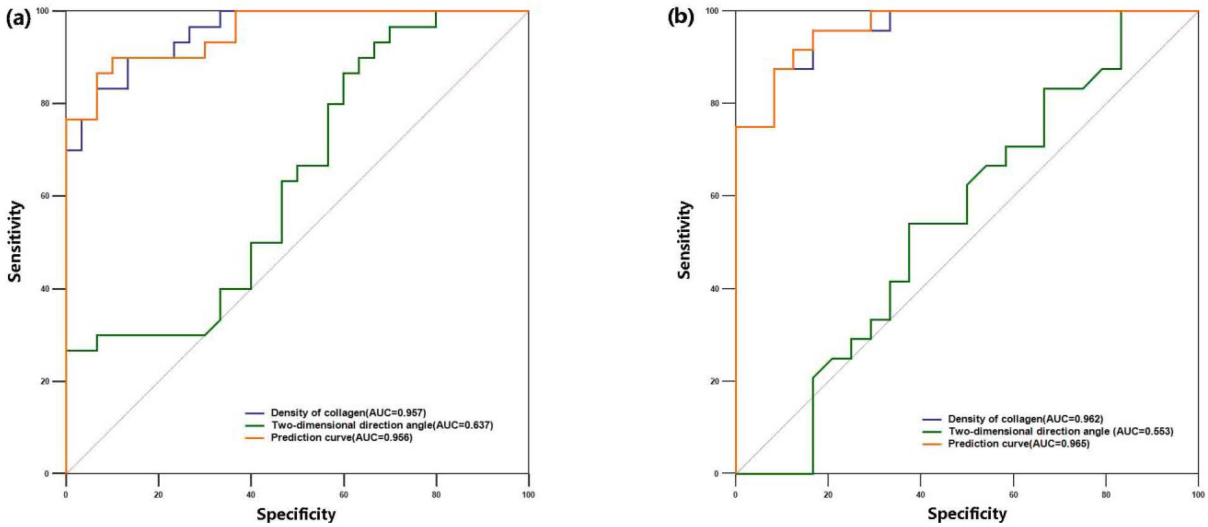

Fig. 7. Comparison of tumor border by ROC curves of the density of the collagen fibers (blue), 2D direction angle of the collagen fibers (green), and predicted value to combine the above two features (orange). (a) ROC curve of cancer cells infiltrating the muscle layer. (b) ROC curve of cancer cells infiltrating the liver.

IV. Conclusion

This work is the first to present a detailed application of MPM for studying HCC. In previous studies on HCC, common factors affecting the prognosis of patients included positive surgical margins [31], lymph node metastasis [32], perineural invasion [33], etc. Among them, complete tumor resection makes the margins negative, which is the only factor controlled by the surgeon. The MPM can be used to assess the condition of the tumor boundary when HCC metastasizes and to provide more theoretical support to ensure that the tumor reaches R0 resection. Our research shows that when cancer cells infiltrate the muscle layer or liver, the MPM can clearly show the morphology of the cells, which is quite different from the normal cells. Moreover, the collagen and elastic fibers of cancerous tissues are significantly different from those of normal tissues, from which the boundaries of the tumor can be easily determined. In addition, it can reflect whether the collagen is degraded or whether there is a fibrotic reaction through the quantitative calculation of the collagen fiber density and the dispersion of the 2D direction angle. Combined with the prediction curve, the tumor boundary can be further determined.

In summary, the MPM was proven to be a potential tool that can not only provide histomorphological features of the HCC for tumor boundary determination, but also help make quantitative diagnosis of the tumor boundary using the prediction curve combining the density and 2D direction angle of the collagen fibers. Therefore, MPM imaging provides a new tool for assessing whether HCC surgery achieves R0 resection.

References

[1] S. Hasegawa, I. Ikai, H. Fujii, E. Hatano, and Y. Shimahara, "Surgical resection of hilar cholangiocarcinoma: Analysis of survival and postoperative complications," *World J. Surg.*, vol. 31, no. 6, pp. 1256–1263, 2007.

[2] Y. Nakanum and Y. Kakuda, "Pathologic classification of cholangiocarcinoma: New concepts," *Best Pract. Res. Clin. Gastroenterol.*, vol. 29, no. 2, pp. 277–293, 2015.

[3] A. V. Fisher and S. M. Ronnekleiv-Kelly, "Surgical management of hilar cholangiocarcinoma," *Curr. Surg. Rep.*, vol. 6, no. 8, pp. 1–16, 2018.

[4] S. M. Hong, A. E. Presley, E. B. Stelow, H. F. Frierson, and C. A. Moskaluk, "Reconsideration of the histologic definitions used in the pathologic staging of extrahepatic bile duct carcinoma," *Amer. J. Surg. Pathol.*, vol. 30, no. 6, pp. 744–749, 2006.

[5] I. Endo et al., "Clinical significance of intraoperative bile duct margin assessment for hilar cholangiocarcinoma," *Ann. Surg. Oncol.*, vol. 15, no. 8, pp. 2104–2112, 2008.

[6] M. L. DeOliveira et al., "Cholangiocarcinoma: Thirty-one-year experience with 564 patients at a single institution," *Ann. Surg.*, vol. 245, no. 5, pp. 755–762, 2007.

[7] N. Akamatsu, Y. Sugawara, and D. Hashimoto, "Surgical strategy for bile duct cancer: Advances and current limitations," *World J. Clin. Oncol.*, vol. 2, no. 2, pp. 94–107, 2011.

[8] W. R. Jarnagin et al., "Staging, resectability, and outcome in 225 patients with hilar cholangiocarcinoma," *Ann. Surg.*, vol. 234, no. 4, pp. 507–519, 2001.

[9] Y. Seyama and M. Makuuchi, "Current surgical treatment for bile duct cancer," *World J. Gastroenterol.*, vol. 13, no. 10, pp. 1505–1515, 2007.

[10] J. Yan et al., "Real-time optical diagnosis for surgical margin in low rectal cancer using multiphoton microscopy," *Surg. Endoscopy*, vol. 28, no. 1, pp. 36–41, 2014.

[11] L. H. Li et al., "Assessment of colloid response by nonlinear optical microscopy after preoperative radiochemotherapy for rectal carcinoma," *J. Biomed. Opt.*, vol. 20, no. 5, 2014, Art. no. 051009.

[12] C. Grappone et al., "Expression of platelet-derived growth factor in newly formed cholangiocytes during experimental biliary fibrosis in rats," *J. Hepatol.*, vol. 31, no. 1, pp. 100–109, 1999.

[13] M. E. Llewellyn, R. P. J. Barretto, S. L. Delp, and M. J. Schnitzer, "Minimally invasive high-speed imaging of sarcomere contractile dynamics in mice and humans," *Nature*, vol. 454, no. 7205, pp. 784–788, 2008.

[14] D. M. Huland et al., "In vivo imaging of unstained tissues using long gradient index lens multiphoton endoscopic systems," *Biomed. Opt. Exp.*, vol. 3, no. 5, pp. 1077–1085, 2012.

[15] D. Chen et al., "Association of the collagen signature in the tumor microenvironment with lymph node metastasis in early gastric cancer," *JAMA Surg.*, vol. 154, no. 3, 2019, Art. no. e185249.

[16] S. Wang et al., "Assessment of tumor invasion depth in colorectal carcinoma using multiphoton microscopy," *IEEE Photon. J.*, vol. 7, no. 2, Apr. 2015, Art. no. 6800808.

[17] S. Wang et al., "Optical visualization of cerebral cortex by label-free multiphoton microscopy," *IEEE J. Sel. Topics Quantum Electron.*, vol. 25, no. 1, pp. 1–8, Jan./Feb. 2019.

[18] J. S. Bredfeldt et al., "Computational segmentation of collagen fibers from second-harmonic generation images of breast cancer," *J. Biomed. Opt.*, vol. 19, no. 1, 2014, Art. no. 16007.

[19] A. M. Stein et al., "An algorithm for extracting the network geometry of three-dimensional collagen gels," *J. Microsc.*, vol. 232, no. 3, pp. 463–475, 2008.
[20] D. E. Henson, J. Albores-Saavedra, and D. Corle, "Carcinoma of the extrahepatic bile ducts. Histologic types, stage of disease, grade, and survival rates," *Cancer*, vol. 70, pp. 1498–1501, 1992.
[21] H. D. Foda and S. Zucker, "Matrix metalloproteinases in cancer invasion, metastasis and angiogenesis," *Drug Discov. Today*, vol. 6, no. 9, pp. 478–482, 2001.
[22] K. J. Chae et al., "Expression of matrix metalloproteinase-2 and -9 and tissue inhibitor of metalloproteinase-1 and -2 in intraductal and nonintraductal growth type of cholangiocarcinoma," *Amer. J. Gastroenterol.*, vol. 99, no. 1, pp. 68–75, 2004.
[23] T. Terada and Y. Nakanuma, "Pathological observations of intrahepatic peribiliary glands in 1000 consecutive autopsy livers. III. Survey of necroinflammation and cystic dilatation," *Hepatology*, vol. 12, no. 5, pp. 1229–1233, 1990.
[24] G. Carpino et al., "Biliary tree stem/progenitor cells in glands of extrahepatic and intraheptic bile ducts: An anatomical in situ study yielding evidence of maturational lineages," *J. Anatomy*, vol. 220, no. 2, pp. 186–199, 2012.
[25] T. Terada and Y. Nakanuma, "Pathological observations of intrahepatic peribiliary glands in 1,000 consecutive autopsy livers. II. A possible source of cholangiocarcinoma," *Hepatology*, vol. 12, pp. 92–97, 1990.
[26] S. M. Zhuo et al., "In vivo, label-free, three-dimensional quantitative imaging of liver surface using multi-photon microscopy," *Appl. Phys. Lett.*, vol. 105, no. 2, 2014, Art. no. 023701.
[27] F. Saffioti et al., "Cholangiocarcinoma is associated with a raised enhanced liver fibrosis score independent of primary sclerosing cholangitis," *Eur. J. Clin. Investigation*, vol. 49, no. 5, 2019, Art. no. e13088.
[28] Y. K. Tao et al., "Assessment of breast pathologi es using nonlinear microscopy," *Proc. Nat. Acad. Sci. USA*, vol. 111, no. 43, pp. 15304–15309, 2014.
[29] J. Tarasińska, "Sample size needed to get given ratio of endpoints for confidence interval of standard deviation in a normal distribution," *Commun. Statist.-Theory Methods*, vol. 46, no. 23, pp. 11480–11484, 2017.
[30] S. Buettner et al., "Conditional probability of long-term survival after resection of hilar cholangiocarcinoma," *HPB*, vol. 18, no. 6, pp. 510–517, 2016.
[31] T. Ebata et al., "Hepatectomy with portal vein resection for hilar cholangiocarcinoma: Audit of 52 consecutive cases," *Ann. Surg.*, vol. 238, no. 5, pp. 720–727, 2003.
[32] S. G. Lee et al., "Surgical treatment of hilar cholangiocarcinoma in the new era: The Asan experience," *J. Hepatobiliary Pancreat*, vol. 17, no. 4, pp. 476–489, 2010.
[33] M. M. R. Bhuiya et al., "Clinicopathologic studies on perineural invasion of bile duct carcinoma," *Ann. Surg.*, vol. 215, no. 4, pp. 344–349, 1992.